Geophysical Research Letters

Spatiotemporal Variations of Riverine Discharge Within the Amazon Basin During the Late Holocene Coincide With Extratropical Temperature Anomalies

D. J. Bertassoli Jr[1] [iD], A. O. Sawakuchi[1] [iD], C. M. Chiessi[2] [iD], E. Schefuß[3], G. A. Hartmann[4] [iD], C. Häggi[3,5], F. W. Cruz[1] [iD], M. Zabel[3] [iD], M. M. McGlue[6], R. A. Santos[1], and F. N. Pupim[7]

[1]Institute of Geosciences, University of São Paulo, São Paulo, Brazil, [2]School of Arts, Sciences and Humanities, University of São Paulo, São Paulo, Brazil, [3]MARUM - Center for Marine Environmental Sciences, Bremen University, Bremen, Germany, [4]Institute of Geosciences, State University of Campinas, Campinas, Brazil, [5]Now at Department of Earth Sciences, University of Southern California, Los Angeles, CA, USA, [6]Department of Earth and Environmental Sciences, University of Kentucky, Lexington, KY, USA, [7]Department of Environmental Sciences, Federal University of São Paulo, Diadema, Brazil

Abstract Late Holocene hydroclimate variations have been extensively recognized in Amazonia, but the effects of such changes on riverine discharge within the Amazon lowlands are still poorly understood. We investigated a sediment core covering circa 4,000 to 300 cal yr BP collected in the lower valley of the Xingu River (Xingu Ria) in an area under the influence of the Amazon River. Our results indicate a decrease in precipitation in the Amazon lowlands throughout the studied period and reduced input of coarser and potassium-rich Amazon River sediments to the confluence from about 2,600 to 1,400 cal yr BP. We suggest that lower temperatures in the extratropical Southern Hemisphere weakened the South American Summer Monsoon and led to a decrease in the water discharge of the Amazon River during this period.

Plain Language Summary The variability of the Amazon River water discharge over the last millennia is still poorly understood. Sediments deposited in the lower valley of the Xingu River, a major eastern tributary of the Amazon River, allowed for the identification of a decrease in rainfall over the Amazon lowlands throughout the last 4,000 years. Changes in the relative input of Amazon and Xingu sediments in an area affected by both rivers indicate that the water discharge of the Amazon River decreased from about 2,600 to 1,400 years ago. We suggest that anomalously low temperatures in the Southern Hemisphere led to drier conditions in Amazonia during this period.

1. Introduction

Precipitation in Amazonia is primarily modulated by variations in the strength of the South American Summer Monsoon (SASM) and by shifts of the Intertropical Convergence Zone (ITCZ, Garreaud et al., 2009; Marengo, 2004). Changes in the sea surface temperatures (SSTs) of the Atlantic and Pacific Oceans severely affect the transport of moisture toward Amazonia and partially control the discharge of the Amazon River and its tributaries (Marengo & Espinoza, 2016). Hydrologic variations in Amazonia have affected local communities and rainforest ecosystems over the last millennia (Cordeiro et al., 2014; Marengo & Espinoza, 2016; Meggers, 1994). As such, it is critical to understand how the Amazon River and its tributaries responded to changes in Amazonian precipitation throughout the late Holocene (i.e., last 4,000 year). Still, deciphering hydroclimatic imbalances in eastern Amazonia is challenging. Speleothems are scarce in this area, and sediment cores collected offshore of the Amazon River mouth may not reveal internal hydrological variability due to the overwhelming Andean signature in the sediment supply (Govin et al., 2014; Höppner et al., 2018). Similarly, autogenic processes such as river avulsions limit comprehensive discussions about water discharge variations based on sediment cores from floodplain lakes (e.g., Aniceto et al., 2014).

In the Xingu River, a major clearwater tributary of the Amazon River, seasonal and tidal oscillations affect water level gradients and modulate flow velocities near its confluence with the Amazon main stem (Fricke et al., 2017). Peak discharge in the Amazon River (about 200,000 m^3/s) occurs when the Xingu River discharge is already at its falling stage (June–July), reversing water level gradients in the confluence zone
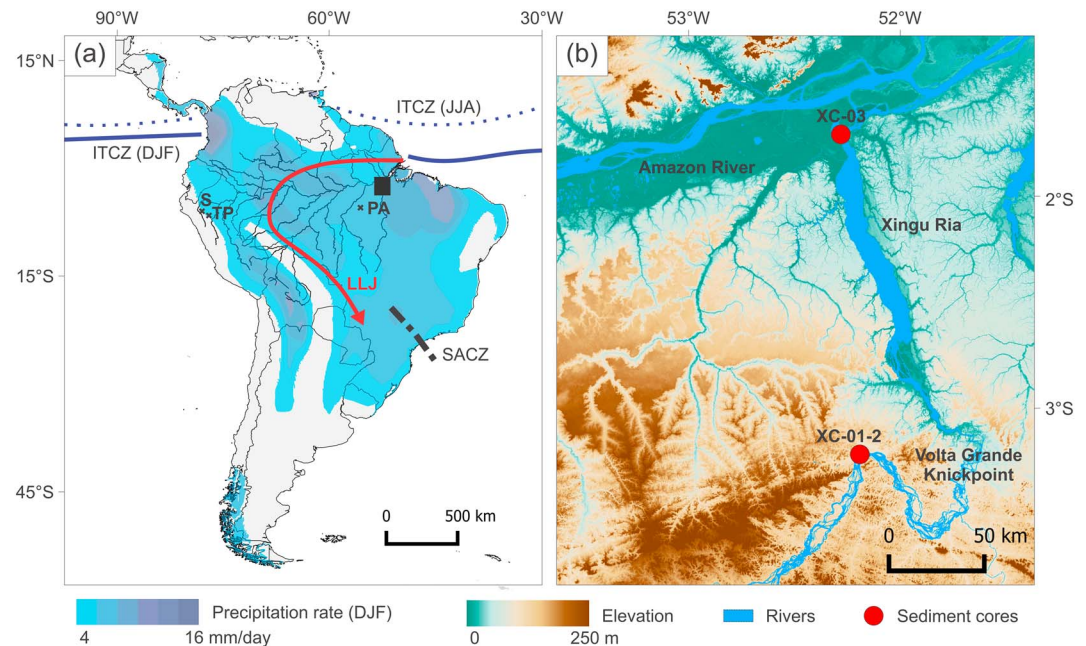
Figure 1. Study area and sampling sites of sediment cores XC-03 and XC-01-2. (a) Schematic representation of the South Atlantic Convergence Zone (SACZ) and ITCZ. The simplified trajectory of the low-level jet (LLJ) is also shown. Blue-shaded areas cover regions with average precipitation rates >4 mm/day during austral summer. The locations of the Paraíso (PA, Wang et al., 2017), Tigre Perdido (TP, van Breukelen et al., 2008), and Shatuca records (S, Bustamante et al., 2016) are also indicated. DJF: December–February; JJA: June–August. A black square depicts the study area detailed in Figure 1b. (b) Digital elevation model of the lower reaches of the Amazon and Xingu rivers (SRTM, Farr et al., 2007) and sites of the studied sediment cores. ITCZ = Intertropical Convergence Zone; SRTM = Shuttle Radar Topography Mission.

(Fricke et al., 2017). Thus, water levels in the lowermost Xingu River are mainly controlled by the Amazon River stage (Figure S1 in the supporting information). Variations in the relative discharge of the Amazon and Xingu Rivers promote barotropic and baroclinic flows that carry Amazon River waters plus sediments into the lower reach of the Xingu River (Fricke et al., 2017). Some of these sediments are deposited in the lake-like Xingu Ria, a broad, drowned incised valley of the Xingu River (Figure 1), and may help to identify hydrologic changes in the catchments of the Amazon and Xingu Rivers (Fricke et al., 2017).

In order to reconstruct regional hydroclimate variability over the last millennia, we investigated a sediment core collected in the lowermost section of the Xingu Ria. We analyzed the hydrogen (δD) and stable carbon (δ¹³C) isotope compositions of long-chain *n*-alkanes to infer changes in paleoprecipitation and vegetation. We also used grain size, magnetic susceptibility, and major elements measured in sediments of the Amazon and Xingu Rivers to reconstruct changes in the relative influx of Amazon River sediments to the Xingu Ria. We compared the obtained results to abrupt changes in a sediment core retrieved from a flood-plain lake outside of the Amazon River influence. Our results provide important insights about relative river discharges in eastern versus western Amazonia throughout the late Holocene.

2. Study Area

The Xingu is a large clearwater river draining eastern Amazonia (Figure 1a). It has a mean annual water discharge of 9,700 m³/s (Latrubesse et al., 2005) and marked seasonality, with discharge varying from 1,000 m³/s (September–October) to 19,000 m³/s (March–April) (Figure S1, ANA, 2017). Whereas rainfall in the Lower Xingu is governed by persistent easterly winds that bring moisture from the Atlantic Ocean, precipitation in the Upper Xingu is strongly related to the SASM (Figure S2, ANA, 2017).

The Xingu River shows a variety of fluvial channel morphologies, with a meandering channel at its upper catchment, a bedrock channel with multiple flow paths at its midportion (Wohl & Merritt, 2001), and a fluvial ria in its downstream section (Archer, 2005). Upstream of the Xingu Ria, a bedrock anastomosing system

known as Volta Grande do Xingu (*Xingu Great Bend*, Figure 1b) comprises channels with rapids flowing above fractured basement rocks (Sawakuchi et al., 2015). Besides being a unique environment for Amazonian biodiversity (Nogueira et al., 2010), those rapids act as a major knickpoint and limit the influence of the Amazon River to upstream portions of the Xingu watershed.

As the Xingu River mainly drains Proterozoic and Archean rocks of the Central Brazilian Shield or their derived-sedimentary cover (de Almeida et al., 1981), topography, weathering conditions, denudation patterns ($6–15 \times 10^{-3}$ mm/year, Sawakuchi et al., 2015; Wittmann et al., 2011), and geological substrates of the Xingu watershed are markedly different from Andean-draining tributaries of the Amazon River (Guyot et al., 2007; Konhauser et al., 1994; Sawakuchi et al., 2018). These distinctions are manifested in the relatively low particulate load and high proportions of stable and conservative elements in both suspended and riverbed sediments of the Xingu River (Bertassoli et al., 2017; Filizola & Guyot, 2009). Thus, it is possible to geochemically trace the influence of Amazon River sediments in the Lower Xingu Ria.

3. Materials and Methods

We investigated two sediment cores (XC-03 and XC-01-2) collected in the Lower Xingu River. XC-03 is a 362-cm-long percussion core obtained from the Xingu Ria, close to the confluence with the Amazon River (01°42′32.12″S, 52°16′47.42″W, Figure 1b). It was retrieved by divers at a water depth of 10 m. The XC-03 core consists of relatively homogeneous fine-grained gray sediments (mainly clay and silt). Sediment core XC-01-2 was retrieved from a seasonally inundated lake within a fluvial island upstream of the Volta Grande knickpoint (03°12′51.40″S, 52°11′24.42″W″, Figure 1b). It is 123-cm long, with the lowermost portion (80–123 cm) composed of medium to coarse sand with fining upward pattern. Fine-grained (silt and clay) brown and dark-gray sediments are dominant in the upper portion (0–80 cm) of XC-01-2. Radiocarbon (^{14}C) ages of the bulk organic fraction (Tables S1 and S2, *n = 7* for XC-03, *n = 4* for XC-01-2) were obtained by Accelerator Mass Spectrometry dating at Beta Analytic Incorporated and Radiocarbon Laboratory of Federal Fluminense University (LAC-UFF). Radiocarbon dating was constrained by the availability of organic material in core XC-01-2, and therefore, the age model for this core is limited to the 20- to 80-cm interval. Further considerations regarding the age models are presented in the supporting information (Text S1).

For long-chain *n*-alkane analysis, approximately 10 g of sediments were collected every 12 cm from core XC-03 and 5 cm from core XC-01-2. The extraction procedure is described in the supporting information (Text S1). The *n*-alkane fraction was analyzed in a Thermo-Fisher Scientific Focus gas chromatograph equipped with a flame ionization detector. Hydrocarbons of different chain lengths were quantified by comparing peak areas of the compounds to external standards. Precision of compound quantification is about 5% based on multiple standard analyses. The carbon preference index (CPI_{25-33}) and the average chain length (ACL_{27-33}) were calculated using the relative distribution of *n*-alkanes (equations are presented in the supporting information, Text S1). The low CPI_{25-33} values obtained from XC-01-2 samples (Figure S5) make interpretations based on compound-specific isotopes impossible for this core. Hence, analyses of δD and $δ^{13}$C of the C_{29} and C_{31} *n*-alkanes were only conducted for core XC-03, which had CPI_{23-33} values generally above 4 (Figure S6).

We analyzed the δD of the C_{29} and C_{31} *n*-alkanes as a proxy for changes in past precipitation (Häggi et al., 2017) on a Thermo-Fisher Scientific MAT 253 isotope ratio mass spectrometer coupled via a GC Isolink operated at 1420 °C to a Thermo-Fisher Scientific Trace GC. Daily determination of the H^+_3 factor varied between 5.1 and 5.2 over the analysis period. All δD analyses were made against calibrated H_2 reference gas, and δD values are reported in per mil against Vienna Standard Mean Ocean Water. Given the investigated period (i.e., late Holocene), an ice volume correction was not required.

Analyses of $δ^{13}$C of long-chain *n*-alkanes, used to reconstruct variations in past vegetation cover (e.g., Castañeda & Schouten, 2011), were carried out on a Thermo-Fisher Scientific MAT 252 isotope ratio mass spectrometer coupled via a GC-C combustion interface with a nickel catalyzer operated at 1000 °C to a Thermo-Fisher Scientific Trace GC. The analyses were conducted against calibrated CO_2 reference gas of known isotopic composition and $δ^{13}$C values are given in per mil against Vienna Pee Dee Belemnite.

Measurements were made in duplicate, and accuracy was controlled for each measurement using the internal squalene standard with known isotopic composition (-180.3 ± 2.3‰ for δD and -19.8 ± 0.2‰ for $\delta^{13}C$). The average values obtained for the internal standard during analyses were -179.5 ± 3.1‰ (δD) and -20.0 ± 0.4‰ ($\delta^{13}C$). Precision was controlled by external n-alkane standards (C_{16} to C_{34},) at every six measurements. Repeated analyses of external n-alkane standards yielded a root-mean-square deviation of 2.2‰ for δD and 0.1‰ for $\delta^{13}C$, respectively. Given the similar behavior of δD values from C_{29} and C_{31} n-alkanes in XC-03 (Figure S7), results are presented as the weighted average of the two compounds (δD C_{29-31}).

We collected sediment aliquots (10 g) from cores XC-03 and XC-01-2 at every 2 cm for grain size and X-ray fluorescence (XRF) analyses ($n = 174$ for XC-03, $n = 40$ for XC-01-2). Grain size distributions of XC-03 samples ($n = 174$) were determined using a laser diffraction particle size analyzer equipped with a wet sample dispersion unit (Malvern Instruments Ltd, Mastersizer 2000 and Hydro 2000 MU). Samples were directly dispersed in 900 mL of deionized water using an ultrasonic bath (one minute) and sodium pyrophosphate as dispersion agent before measurements. Precision standards for this method are described in Miller and Schaetzl (2012).

Samples for XRF analyses were dried, ground, and sealed in inert sample cups covered with ultrathin Mylar. Measurements were made using a Bruker Titan S1 handheld XRF device (6–50 kV, 4.5–195 μA) for XC-03 and a Bruker Tracer IV-SD handheld energy-dispersive XRF (40 kV, 60 μA) for XC-01-2. Individual XRF scans were made over 60 s for XC-03 and 90 s for XC-01-2. Internal consistency was verified by routine scanning of a standard. The coefficient of variation was below 5.0% for all analyzed elements (i.e., Al, Si, K, Ti, Fe, and Mn).

We also retrieved 141 samples from XC-03 using cubic plastic boxes (8 cm^3) placed side-by-side for magnetic susceptibility measurements. Low-field magnetic susceptibility of discrete samples was measured using an Agico Kappabridge MFK1-FA system under different frequencies (976 and 15616 Hz) in a 200 A/m field at room temperature (e.g., Dearing et al., 1996; Ustra et al., 2018). Frequency-dependent susceptibility ($\chi fd\%$) was calculated from the difference between low- and high-frequency susceptibility values, enabling an evaluation of the spectrum of grain sizes of single domain to superparamagnetic grains in the samples. Individual results were mass normalized, and coefficient of variation was below 0.5% for the analyzed frequencies.

4. Results and Discussion

4.1. Age Models

The age model of core XC-03 suggests no major changes in sediment accumulation and covers the period from circa 4,000 to 300 cal yr BP (Figure S3). Sedimentation rates range from 0.5 to 1.4 mm/year and yield an average temporal resolution of 20 years for geochemical, grain size, and magnetic susceptibility records. Grain size and major element distribution do not show abrupt shifts that could indicate hiatuses in accumulation (Figures S9 and S10).

Core XC-01-2 responds exclusively to the sediment supply and hydrology of the Xingu River watershed. These results differ from XC-03, which provides direct information on the sediment supplies from both Amazon and Xingu Rivers. Ages obtained from core XC-01-2 span from circa 2,800 to 400 cal yr BP (Figure S4). Sedimentation rates are, on average, significantly lower than in the Xingu Ria, varying from about 0.14 to 0.77 mm/year in the upper deposit (0- to 80-cm depth).

4.2. Amazon Lowlands Precipitation During the Late Holocene

Analyses of the organic fraction show that C_{29} and C_{31} are the dominant n-alkanes in core XC-03, with respective average concentrations of 0.4 ± 0.1 and 0.5 ± 0.2 μg/g (dry sediment). The XC-03 record presents average $\delta^{13}C$ of -33.7 ± 0.3‰ for C_{29} and -34.5 ± 0.2‰ for C_{31} and shows constant dominance of C_3 vegetation throughout the late Holocene (Figure 2d). Riverbed sediments from the Amazon main stem and Andean tributaries exhibit more ^{13}C-enriched signatures (average $\delta^{13}C$ between -35 and -33‰) than the Xingu River (average $\delta^{13}C$ more depleted than -35‰, Häggi et al., 2016). The $\delta^{13}C$ of n-alkanes from XC-03 differs from the typical signatures of the Xingu River sediments and suggests that the organic material reaching the studied site is predominantly derived from the Amazon River. The weighted average of δD from
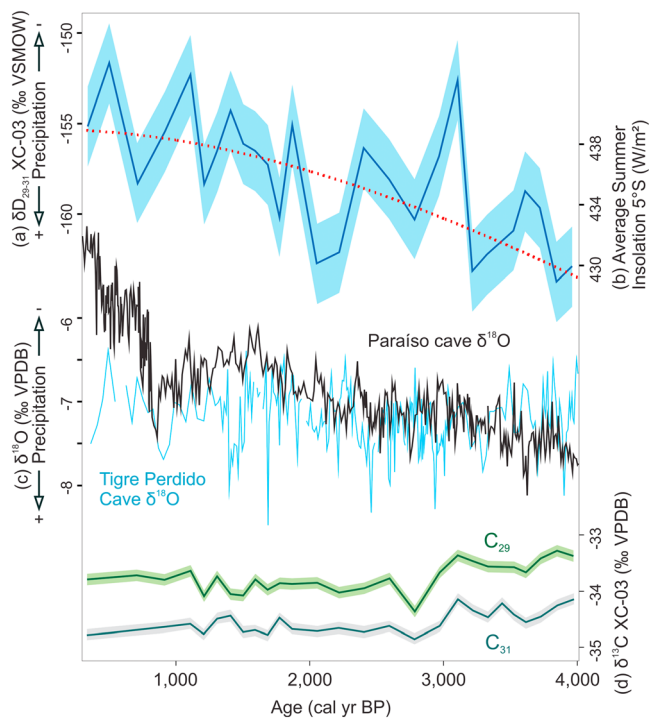
Figure 2. Paleoenvironmental proxies from core XC-03 in the Xingu-Amazon Rivers confluence compared to Amazonian speleothems records. (a) Weighted average of the δD of long-chain *n*-alkanes (C_{29} and C_{31}) from core XC-03. (b) Average austral summer insolation at 5°S (Laskar et al., 2004) (c) Speleothem $\delta^{18}O$ records from Paraíso Cave (black, Wang et al., 2017) and from Tigre Perdido Cave (light blue, van Breukelen et al 2008), as proxies for precipitation over eastern and western Amazonia, respectively. (d) $\delta^{13}C$ of *n*-alkanes C_{29} and C_{31} from core XC-03, values are relatively stable and indicate a strong dominance of C3 vegetation. In Figures 2a and 2d, shaded areas represent the 2σ uncertainty envelope of isotopic values obtained by repeated analyses of external *n*-alkane standards.

XC-03 C_{29} and C_{31} *n*-alkanes ranges from about −151 to −163‰, with a slight trend of increasing values toward the present (Figure 2a). The δD results are also within the range presented by Häggi et al. (2016) for riverbed samples from the Amazon River (−152 to −165‰).

Plant leaf waxes in sediments of the Amazon River are spatially integrated (Feakins et al., 2018), and the Amazon lowlands are the dominant source area of organic material and plant waxes to the lower Amazon River (Bouchez et al., 2014; Häggi et al., 2016; Ponton et al., 2014). Hence, we interpret the δD C_{29-31} record from XC-03 to represent δD variations of regional meteoric water, which are mainly controlled by the precipitation amount in the Amazon lowlands (Häggi et al., 2016, 2017).

Considering that XC-03 $\delta^{13}C$ values point to a relatively stable vegetation cover (Figure 2d), we assume that evapo-transpirative enrichment and changes in vegetation metabolism and sediment sourcing did not exert a significant effect on the δD values of long-chain *n*-alkanes variability through the late Holocene. The stable ACL_{27-33} (30.2 ± 0.1) and CPI_{25-33} (4.4 ± 0.2.) in XC-03 sediments suggest that degradation and input of petrogenic (fossil) material also have insignificant effects on the δD C_{29-31} and $\delta^{13}C$ records (Figure S6).

The XC-03 δD C_{29-31} record suggests that eastern Amazonia (i.e., the Amazon lowlands) experienced a decrease in precipitation throughout the late Holocene (Figure 2a). These results follow an increase in average austral summer insolation (Figure 2b) and differ from paleoprecipitation records from the Andes and western Amazonia (e.g., Figure 2c, Baker et al., 2001). The antiphase variability behavior between eastern and western Amazonia on the orbital time scale has been interpreted as a product of an increased sea-land thermal gradient and atmospheric convection (Cheng et al., 2013).

Both the XC-03 δD C_{29-31} and Paraíso Cave $\delta^{18}O$ records (Figures 2a and 2c) suggest that a trend of decreasing humidity prevailed in a significant part of the Amazon lowlands during the late Holocene. Western Amazonian (Andean) precipitation is relatively stable during this period (Figure 2c, Bird et al., 2011), highlighting persistent heterogeneous precipitation trends among different regions of the Amazon Basin. The contrasting east-west precipitation trends are also evident in neodymium isotopic record, which suggest a shift in the Amazon River sediment supply toward a greater Andes-dominated signal during the late Holocene (Höppner et al., 2018).

4.3. Multicentennial Anomalies on the Discharge of the Amazon and Xingu Rivers

Variations in grain size, major elements, and χfd% in core XC-03 (Figure 3b–3d) suggest significant changes in the relative sediment supply of the Amazon and Xingu Rivers to the Xingu Ria. The percentage of fine-grained sediments and Fe/K ratios in XC-03 increases after 3,600 cal yr BP and reaches maximum values between 2,600 and 1,400 cal yr BP (Figures 3b and 3d). A marked increase in χfd% around 2,700 yr BP agrees with most of the changes in the distribution of major elements and grain size (Figure 3c). A synchronous shift in magnetic susceptibility and Si/Al is also evident in core XC-01-2 (Figures S12 and 3a).

Fe/K values have been used as a provenance proxy for distinguishing sediments from the Amazon River main stem and lowland-draining tributaries (Govin et al., 2014; Häggi et al., 2016). Modern riverbed and suspended sediments from the Amazon River present Fe/K values around 2, while sediments from the Xingu River range from 3 to 27, depending on season (Bertassoli et al., 2017; Sawakuchi et al., 2018; Zhang et al., 2017). Thus, the increase in Fe/K values, frequency-dependent magnetic susceptibility, and silt and clay content in XC-03 indicates diminished relative proportions of coarser Amazon River sediments reaching the studied site (Figures 3b–3d).
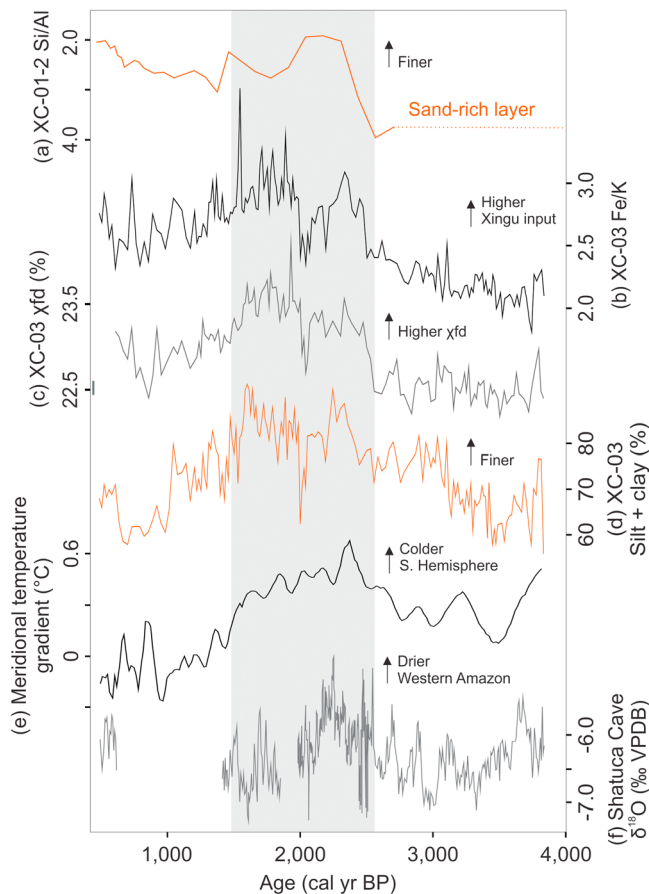
Figure 3. Comparison of the XC-03 and XC-01-2 records with other paleoclimate records. Si/Al values in core XC-01-2 (a) and XC-03 Fe/K values (b), frequency-dependent magnetic susceptibility (c), and fine-grained (silt and clay) sediment content (d). (e) Extratropical temperature gradient between the Northern and Southern Hemispheres (Marcott et al., 2013) (f) Speleothem δ¹⁸O record from Shatuca Cave, representing changes in precipitation in the northeastern flank of the Peruvian Andes in western Amazonia (Bustamante et al., 2016). The gray vertical bar highlights coincident shifts in the depicted records.

Although fluctuations in the weathering intensity of sediment sources could have affected geochemical XC-03 records, we deem this process less probable of producing the described trends. Indeed, variations in Fe/K values of Amazon River sediments obtained by Zhang et al. (2017) during periods of major changes in western Amazonian precipitation (Heinrich and Dansgaard-Oeschger stadials) were rather subtle when compared to the fluctuations in our data. Potential effects of major late Holocene physiographic changes on sediment grain size and Fe/K values are unlikely, considering the correspondence between changes recorded in cores XC-03 and XC-01-2 and other regional paleoclimate records (e.g., Figure S13). Additionally, the lower portion of the Xingu Ria is bound by stable Pleistocene terraces (Pupim et al., 2016), precluding major variations in channel morphology during the Holocene.

We interpret that periods of reduced contribution of Amazon River sediments to the XC-03 site can be caused by two processes: (i) a diminished efficiency of the backwater effect in the confluence of the Amazon and Xingu Rivers; and (ii) a more downstream position of the mixing zone of Amazon and Xingu waters, which would increase the distance of the XC-03 site from the confluence. Both processes are modulated by changes in the Amazon/Xingu discharge ratios (Best, 1988; Dixon et al., 2018) and suggest a decrease in the Amazon River discharge relative to the discharge of the Xingu River from 2,600 to 1,400 cal yr BP.

Riverbed sediments in Amazon rivers show a strong positive correlation between Si/Al values and grain size that reflects the proportion of aluminum-rich clay minerals in relation to silicon-rich sand (Bouchez et al., 2011; Sun et al., 2017). A shift toward lower Si/Al values in XC-01-2 (Figure 3a) indicates that at about 2,700 cal yr BP, sand bar deposits were superimposed by aluminum-rich fine-grained lacustrine sediments. The observed grain size pattern is synchronous to an increase in magnetic susceptibility (Figure S12) and consistent with the establishment of calm water conditions atop a stabilized sand bar depression during an interval of decreased discharge of the Xingu River. The synchronicity of major geochemical changes in XC-03 and XC-01-2 from 2,600 to 1,400 cal yr BP indicates that although the discharge of the Amazon mainstem decreased relative to the Xingu River, the discharge of both rivers were likely lower during this period (Figures 3a–3d).

The anomalies seen in cores XC-03 and XC-01-2 coincide with multicentennial dry events and a slight shift in precipitation trends in western Amazonia (e.g., Figure 3f, Bird et al., 2011; Bustamante et al., 2016; Kanner et al., 2013). Thus, decreased SASM intensity from 2,600 to 1,400 cal yr BP may have contributed to anomalous water discharges in the Amazon and Xingu Rivers, affecting their sediment loads and relative discharge ratios. This, in turn, dampened the backwater effect and possibly moved the mixing zone of the Amazon and Xingu Rivers toward a more downstream position.

The correspondence of the XC-03 and Shatuca cave δ¹⁸O records with the reconstructed hemispheric temperature gradient (Marcott et al., 2013) suggests that the meridional temperature gradient was an important forcing of changes in SASM intensity during the late Holocene (Figures 3b–3f). Importantly, most of the variability controlling the negative anomaly in the meridional temperature gradient from 2,600 to 1,400 cal yr BP (Figure 3e) is related to anomalous multicentennial cold events in Antarctica and the Southern Ocean (Figure S13, Bentley et al., 2009; Nielsen et al., 2004; Masson et al., 2000; Rosqvist & Schuber, 2003; Shevenell et al., 2011). The teleconnections of extratropical cooling and tropical rainfall intensity mediated by interhemispheric thermal gradients are thoroughly discussed in Chiang and Friedman (2012).

Although previous studies have mainly focused on North Atlantic SST variability forcing on SASM intensity, our data suggest that extratropical South Hemisphere temperatures may also have played an important role

in controlling Amazonian rainfall patterns during the late Holocene. More specifically, the negative anomaly of the meridional temperature gradient (Figure 3e) would produce a northward displacement of the ITCZ or a limitation of the seasonal southward migration of the ITCZ during austral summer (Figure S14, Schneider et al., 2014), significantly decreasing precipitation in western Amazonia. Indeed, several Caribbean records suggest a more stable northern position of the ITCZ from about 2,400 to 1,250 cal yr BP (e.g., Figure S13, Donnelly & Woodruff, 2007; Malaizé et al., 2011).

Variations in the meridional temperature gradient promoted spatially heterogeneous rainfall changes over different time scales in the Amazon Basin (i.e., Chiessi et al., 2009; Marengo et al., 2008; Zhang et al., 2017). In 2005, an anomalous northward displacement of the ITCZ linked to warmer SST in the tropical North Atlantic contributed to one of the most intense droughts recorded in western Amazonia (Marengo et al., 2008; Panisset et al., 2018; Zeng et al., 2008). During this event, while western tributaries of the Amazon River had their water discharges dramatically reduced, tributaries of central and eastern Amazonia were marginally affected (Marengo et al., 2008). Considering the recent trend toward more intense droughts in Amazonia (Lopes et al., 2016), the anomalous conditions from 2,600 to 1,400 cal yr BP may serve as an important analog to understand the impacts of future droughts in a changing climate. Additionally, our findings can contribute to discussions regarding the impact of multicentennial climatic events in technological changes and in the regional increase in human activity and socio-political complexity around 2,500–2,000 cal yr BP in Amazonia (Heckenberger & Neves, 2009; Maezumi et al., 2018).

5. Conclusions

Our results show that sediments accumulated in Amazonian fluvial rias provide useful information to disentangle the response of the Amazon River and its tributaries to hydrological changes during the late Holocene. The δD $C_{29\text{-}31}$ record from core XC-03 suggests an overall drying trend in the Amazon lowlands throughout the last 4,000 years that contrasts with western Amazonian precipitation proxies. The marked increase (decrease) in Fe/K (grain size) from 2,600 to 1,400 cal yr BP indicates relatively lower input of Amazon River sediments into the Xingu Ria and reveals a multicentennial dry event in Amazonia that departs from the insolation-controlled trend. We suggest that changes in the meridional temperature gradient linked to lower temperatures in the extratropical Southern Hemisphere sustained a more northern position of the ITCZ from 2,600 to 1,400 cal yr BP. This, in turn, weakened SASM-related rainfall in Amazonia and decreased the discharge of the Amazon River relative to the discharge of the Xingu River during this period. Our records document spatially heterogeneous rainfall changes in Amazonia linked to insolation and interhemispheric temperature anomalies.

References

ANA. (2017). Hidroweb: Sistema de Informações Hidrológicas. Retrieved in August 1, 2017 from http://www.snirh.gov.br/hidroweb/.

Aniceto, K., Moreira-Turcq, P., Cordeiro, R. C., Fraizy, P., Quintana, I., & Turcq, B. (2014). Holocene paleohydrology of Quistococha Lake (Peru) in the upper Amazon Basin: Influence on carbon accumulation. *Palaeogeography, Palaeoclimatology, Palaeoecology*, 415, 165–174. https://doi.org/10.1016/j.palaeo.2014.08.018

Archer, A. W. (2005). Review of Amazonian depositional systems. In *Fluvial Sedimentology VII*, (pp. 17–39). Oxford, UK: Blackwell Publishing Ltd. https://doi.org/10.1002/9781444304350.ch2

Baker, P. A., Seltzer, G. O., Fritz, S. C., Dunbar, R. B., Grove, M. J., Tapia, P. M., et al. (2001). The history of South American tropical precipitation for the past 25,000 years. *Science*, 291(5504), 640–643. https://doi.org/10.1126/science.291.5504.640

Bentley, M. J., Hodgson, D. A., Smith, J. A., Cofaigh, C. Ó., Domack, E. W., Larter, R. D., et al. (2009). Mechanisms of Holocene palaeoenvironmental change in the Antarctic Peninsula region. *Holocene*, 19(1), 51–69. https://doi.org/10.1177/0959683608096603

Bertassoli, D. J., Sawakuchi, A. O., Sawakuchi, H. O., Pupim, F. N., Hartmann, G. A., McGlue, M. M., et al. (2017). The fate of carbon in sediments of the Xingu and Tapajós Clearwater Rivers, Eastern Amazon. *Frontiers in Marine Science*, 4. https://doi.org/10.3389/fmars.2017.00044

Best, J. L. (1988). Sediment transport at river channel confluences. *Sedimentology*, 35(3), 481–498. https://doi.org/10.1111/j.1365-3091.1988.tb00999.x

Bird, B. W., Abbott, M. B., Rodbell, D. T., & Vuille, M. (2011). Holocene tropical South American hydroclimate revealed from a decadally resolved lake sediment $\delta^{18}O$ record. *Earth and Planetary Science Letters*, 310(3–4), 192–202. https://doi.org/10.1016/j.epsl.2011.08.040

Bouchez, J., Gaillardet, J., France-Lanord, C., Maurice, L., & Dutra-Maia, P. (2011). Grain size control of river suspended sediment geochemistry: Clues from Amazon River depth profiles. *Geochemistry, Geophysics, Geosystems*, 12, Q03008. https://doi.org/10.1029/2010GC003380

Bouchez, J., Galy, V., Hilton, R. G., Gaillardet, J., Moreira-Turcq, P., Pérez, M. A., et al. (2014). Source, transport and fluxes of Amazon River particulate organic carbon: Insights from river sediment depth-profiles. *Geochimica et Cosmochimica Acta*, 133, 280–298. https://doi.org/10.1016/j.gca.2014.02.032

Bustamante, M. G., Cruz, F. W., Vuille, M., Apaéstegui, J., Strikis, N., Panizo, G., et al. (2016). Holocene changes in monsoon precipitation in the Andes of NE Peru based on d18O speleothem records. *Quaternary Science Reviews*, *146*, 274–287. https://doi.org/10.1016/j.quascirev.2016.05.023

Castañeda, I. S., & Schouten, S. (2011). A review of molecular organic proxies for examining modern and ancient lacustrine environments. *Quaternary Science Reviews*, *30*(21–22), 2851–2891. https://doi.org/10.1016/j.quascirev.2011.07.009

Cheng, H., Sinha, A., Cruz, F. W., Wang, X., Edwards, R. L., D'Horta, F. M., et al. (2013). Climate change patterns in Amazonia and biodiversity. *Nature Communications*, *4*(1), 1411. https://doi.org/10.1038/ncomms2415

Chiang, J. C., & Friedman, A. R. (2012). Extratropical cooling, interhemispheric thermal gradients, and tropical climate change. *Annual Review of Earth and Planetary Sciences*, *40*(1), 383–412. https://doi.org/10.1146/annurev-earth-042711-105545

Chiessi, C. M., Mulitza, S., Pätzold, J., Wefer, G., & Marengo, J. A. (2009). Possible impact of the Atlantic Multidecadal Oscillation on the South American summer monsoon. *Geophysical Research Letters*, *36*, L21707. https://doi.org/10.1029/2009GL039914

Cordeiro, R. C., Turcq, B., Moreira, L. S., Rodrigues, R., de Aragão, R., Lamego Simões Filho, F. F., et al. (2014). Palaeofires in Amazon: Interplay between land use change and palaeoclimatic events. *Palaeogeography, Palaeoclimatology, Palaeoecology*, *415*, 137–151. https://doi.org/10.1016/j.palaeo.2014.07.020

de Almeida, F. F. M., Hasui, Y., de Brito Neves, B. B., & Fuck, R. A. (1981). Brazilian structural provinces: An introduction. *Earth-Science Reviews*, *17*(1-2), 1–29. https://doi.org/10.1016/0012-8252(81)90003-9

Dearing, J. A., Dann, R. J. L., Hay, K., Lees, J. A., Loveland, P. J., Maher, B. A., & O'grady, K. (1996). Frequency-dependent susceptibility measurements of environmental materials. *Geophysical Journal International*, *124*(1), 228–240. https://doi.org/10.1111/j.1365-246X.1996.tb06366.x

Dixon, S. J., Sambrook, S. G. H., Best, J. L., Nicholas, A. P., Bull, J. M., Vardy, M. E., et al. (2018). The planform mobility of river channel confluences: Insights from analysis of remotely sensed imagery. *Earth-Science Reviews*, *176*, 1–18. https://doi.org/10.1016/j.earscirev.2017.09.009

Donnelly, J. P., & Woodruff, J. D. (2007). Intense hurricane activity over the past 5,000 years controlled by El Niño and the West African monsoon. *Nature*, *447*(7143), 465–468. https://doi.org/10.1038/nature05834

Farr, T. G., Rosen, P. A., Caro, E., Crippen, R., Duren, R., Hens-ley, S., et al. (2007). The shuttle radar topography mission. *Reviews of Geophysics*, *45*, RG2004. https://doi.org/10.1029/2005RG000183

Feakins, S. J., Wu, M. S., Ponton, C., Galy, V., & West, A. J. (2018). Dual isotope evidence for sedimentary integration of plant wax biomarkers across an Andes-Amazon elevation transect. *Geochimica et Cosmochimica Acta*, *242*, 64–81. https://doi.org/10.1016/j.gca.2018.09.007

Filizola, N., & Guyot, J. L. (2009). Suspended sediment yields in the Amazon basin: An assessment using the Brazilian national data set. *Hydrological Processes*, *23*(22), 3207–3215. https://doi.org/10.1002/hyp.7394

Fricke, A. T., Nittrouer, C. A., Ogston, A. S., Nowacki, D. J., Asp, N. E., Souza Filho, P. W. M., & da Silva, M. S. (2017). River tributaries as sediment sinks: Processes operating where the Tapajós and Xingu Rivers meet the Amazon tidal river. *Sedimentology*, *64*(6), 1731–1753. https://doi.org/10.1111/sed.12372

Garreaud, R. D., Vuille, M., Compagnucci, R., & Marengo, J. (2009). Present-day South American climate. *Palaeogeography, Palaeoclimatology, Palaeoecology*, *281*(3–4), 180–195. https://doi.org/10.1016/j.palaeo.2007.10.032

Govin, A., Chiessi, C. M., Zabel, M., Sawakuchi, A. O., Heslop, D., Hörner, T., et al. (2014). Terrigenous input off northern South America driven by changes in Amazonian climate and the North Brazil Current retroflection during the last 250 ka. *Climate of the Past*, *10*(2), 843–862. https://doi.org/10.5194/cp-10-843-2014

Guyot, J. L., Jouanneau, J. M., Soares, L., Boaventura, G. R., Maillet, N., & Lagane, C. (2007). Clay mineral composition of river sediments in the Amazon Basin. *Catena*, *71*(2), 340–356. https://doi.org/10.1016/j.catena.2007.02.002

Häggi, C., Chiessi, C. M., Merkel, U., Mulitza, S., Prange, M., Schulz, M., & Schefuß, E. (2017). Response of the Amazon rainforest to late Pleistocene climate variability. *Earth and Planetary Science Letters*, *479*, 50–59. https://doi.org/10.1016/j.epsl.2017.09.013

Häggi, C., Sawakuchi, A. O., Chiessi, C. M., Mulitza, S., Mollenhauer, G., Sawakuchi, H. O., et al. (2016). Origin, transport and deposition of leaf-wax biomarkers in the Amazon Basin and the adjacent Atlantic. *Geochimica et Cosmochimica Acta*, *192*, 149–165. https://doi.org/10.1016/j.gca.2016.07.002

Heckenberger, M., & Neves, E. G. (2009). Amazonian archaeology. *Annual Review of Anthropology*, *38*(1), 251–266. https://doi.org/10.1146/annurev-anthro-091908-164310

Höppner, N., Lucassen, F., Chiessi, C. M., Sawakuchi, A. O., & Kasemann, S. A. (2018). Holocene provenance shift of suspended particulate matter in the Amazon River basin. *Quaternary Science Reviews*, *190*, 66–80. https://doi.org/10.1016/j.quascirev.2018.04.021

Kanner, L. C., Burns, S. J., Cheng, H., Edwards, R. L., & Vuille, M. (2013). High-resolution variability of the South American summer monsoon over the last seven millennia: Insights from a speleothem record from the central Peruvian Andes. *Quaternary Science Reviews*, *75*, 1–10. https://doi.org/10.1016/j.quascirev.2013.05.008

Konhauser, K. O., Fyfe, W. S., & Kronberg, B. I. (1994). Multi-element chemistry of some Amazonian waters and soils. *Chemical Geology*, *111*(1–4), 155–175. https://doi.org/10.1016/0009-2541(94)90088-4

Laskar, J., Robutel, P., Joutel, F., Gastineau, M., Correia, A. C. M., & Levrard, B. (2004). A long-term numerical solution for the insolation quantities of the Earth. *Astronomy and Astrophysics*, *428*(1), 261–285. https://doi.org/10.1051/0004-6361:20041335

Latrubesse, E. M., Stevaux, J. C., & Sinha, R. (2005). Tropical rivers. *Geomorphology*, *70*(3–4), 187–206. https://doi.org/10.1016/j.geomorph.2005.02.005

Lopes, A. V., Chiang, J. C. H., Thompson, S. A., & Dracup, J. A. (2016). Trend and uncertainty in spatial-temporal patterns of hydrological droughts in the Amazon basin. *Geophysical Research Letters*, *43*, 3307–3316. https://doi.org/10.1002/2016GL067738

Maezumi, S. Y., Alves, D., Robinson, M., de Souza, J. G., Levis, C., Barnett, R. L., et al. (2018). The legacy of 4,500 years of polyculture agroforestry in the eastern Amazon. *Nature Plants*, *4*(8), 540–547. https://doi.org/10.1038/s41477-018-0205-y

Malaizé, B., Bertran, P., Carbonel, P., Bonnissent, D., Charlier, K., Galop, D., et al. (2011). Hurricanes and climate in the Caribbean during the past 3700 years BP. *Holocene*, *21*(6), 911–924. https://doi.org/10.1177/0959683611400198

Marcott, S. A., Shakun, J. D., Clark, P. U., & Mix, A. C. (2013). A reconstruction of regional and global temperature for the past 11,300 years. *Science*, *339*(6124), 1198–1201. https://doi.org/10.1126/science.1228026

Marengo, J. A. (2004). Interdecadal variability and trends of rainfall across the Amazon basin. *Theoretical and Applied Climatology*, *78*(1–3), 79–96. https://doi.org/10.1007/s00704-004-0045-8

Marengo, J. A., & Espinoza, J. C. (2016). Extreme seasonal droughts and floods in Amazonia: Causes, trends and impacts. *International Journal of Climatology*, *36*(3), 1033–1050. https://doi.org/10.1002/joc.4420

Marengo, J. A., Nobre, C. A., Tomasella, J., Cardoso, M. F., & Oyama, M. D. (2008). Hydro-climatic and ecological behaviour of the drought of Amazonia in 2005. *Philosophical Transactions of the Royal Society, B: Biological Sciences*, *363*(1498), 1773–1778. https://doi.org/10.1098/rstb.2007.0015

Masson, V., Vimeux, F., Jouzel, J., Morgan, V., Delmotte, M., Ciais, P., et al. (2000). Holocene climate variability in Antarctica based on 11 ice-core isotopic records. *Quaternary Research*, *54*(3), 348–358. https://doi.org/10.1006/qres.2000.2172

Meggers, B. J. (1994). Archeological evidence for the impact of mega-Niño events on Amazonia during the past two millennia. *Climatic Change*, *28*(4), 321–338. https://doi.org/10.1007/BF01104077

Miller, B. A., & Schaetzl, R. J. (2012). Precision of soil particle size analysis using laser diffractometry. *Soil Science Society of America Journal*, *76*(5), 1719–1727. https://doi.org/10.2136/sssaj2011.0303

Nielsen, S. H. H., Koç, N., & Crosta, X. (2004). Holocene climate in the Atlantic sector of the Southern Ocean: Controlled by insolation or oceanic circulation? *Geology*, *32*(4), 317–320. https://doi.org/10.1130/G20334.1

Nogueira, C., Buckup, P. A., Menezes, N. A., Oyakawa, O. T., Kasecker, T. P., Neto, M. B. R., & da Silva, J. M. C. (2010). Restricted-range fishes and the conservation of Brazilian freshwaters. *PLoS ONE*, *5*(6), 1–10. https://doi.org/10.1371/journal.pone.0011390

Panisset, J. S., Libonati, R., Gouveia, C. M. P., Machado-Silva, F., França, D. A., França, J. R. A., & Peres, L. F. (2018). Contrasting patterns of the extreme drought episodes of 2005, 2010 and 2015 in the Amazon Basin. *International Journal of Climatology*, *38*(2), 1096–1104. https://doi.org/10.1002/joc.5224

Ponton, C., West, A. J., Feakins, S. J., & Galy, V. (2014). Leaf wax biomarkers in transit record river catchment composition. *Geophysical Research Letters*, *41*, 6420–6427. https://doi.org/10.1002/2014GL061328

Pupim, F. N., Sawakuchi, A. O., Mineli, T. D., & Nogueira, L. (2016). Evaluating isothermal thermoluminescence and thermally transferred optically stimulated luminescence for dating of Pleistocene sediments in Amazonia. *Quaternary Geochronology*, *36*, 28–37. https://doi.org/10.1016/j.quageo.2016.08.003

Rosqvist, G. C., & Schuber, P. (2003). Millennial-scale climate changes on south Georgia, Southern Ocean. *Quaternary Research*, *59*(3), 470–475. https://doi.org/10.1016/S0033-5894(03)00036-X

Sawakuchi, A. O., Hartmann, G. A., Sawakuchi, H. O., Pupim, F. N., Bertassoli, D. J., Parra, M., et al. (2015). The Volta Grande do Xingu: Reconstruction of past environments and forecasting of future scenarios of a unique Amazonian fluvial landscape. *Scientific Drilling*, *20*, 21–32. https://doi.org/10.5194/sd-20-21-2015

Sawakuchi, A. O., Jain, M., Mineli, T. D., Nogueira, L., Bertassoli, D. J., Häggi, C., et al. (2018). Luminescence of quartz and feldspar fingerprints provenance and correlates with the source area denudation in the Amazon River basin. *Earth and Planetary Science Letters*, *492*, 152–162. https://doi.org/10.1016/j.epsl.2018.04.006

Schneider, T., Bischoff, T., & Haug, G. H. (2014). Migrations and dynamics of the intertropical convergence zone. *Nature*, *513*(7516), 45–53. https://doi.org/10.1038/nature13636

Shevenell, A. E., Ingalls, A. E., Domack, E. W., & Kelly, C. (2011). Holocene Southern Ocean surface temperature variability west of the Antarctic Peninsula. *Nature*, *470*(7333), 250–254. https://doi.org/10.1038/nature09751

Sun, S., Schefuß, E., Mulitza, S., Chiessi, C. M., Sawakuchi, A. O., Zabel, M., et al. (2017). Origin and processing of terrestrial organic carbon in the Amazon system: Lignin phenols in river, shelf, and fan sediments. *Biogeosciences*, *14*(9), 2495–2512. https://doi.org/10.5194/bg-14-2495-2017

Ustra, A., Mendonça, C. A., Leite, A., Jovane, L., & Trindade, R. I. F. (2018). Quantitative interpretation of the magnetic susceptibility frequency dependence. *Geophysical Journal International*, *213*(2), 805–814. https://doi.org/10.1093/gji/ggy007

van Breukelen, M. R., Vonhof, H. B., Hellstrom, J. C., Wester, W. C. G., & Kroon, D. (2008). Fossil dripwater in stalagmites reveals Holocene temperature and rainfall variation in Amazonia. *Earth and Planetary Science Letters*, *275*(1–2), 54–60. https://doi.org/10.1016/j.epsl.2008.07.060

Wang, X., Lawrence Edwards, R., Auler, A. S., Cheng, H., Kong, K., Wang, Y., et al. (2017). Hydroclimate changes across the Amazon lowlands over the past 45,000 years. *Nature*, *541*(7636), 204–207. https://doi.org/10.1038/nature20787

Wittmann, H., von Blanckenburg, F., Maurice, L., Guyot, J. L., Filizola, N., & Kubik, P. W. (2011). Sediment production and delivery in the Amazon River basin quantified by in situ-produced cosmogenic nuclides and recent river loads. *Bulletin of the Geological Society of America*, *123*(5-6), 934–950. https://doi.org/10.1130/B30317.1

Wohl, E. E., & Merritt, D. M. (2001). Bedrock channel morphology. *Geological Society of America Bulletin*, *113*(9), 1205–1212. https://doi.org/10.1130/0016-7606(2001)113<1205

Zeng, N., Yoon, J. H., Marengo, J. A., Subramaniam, A., Nobre, C. A., Mariotti, A., & Neelin, J. D. (2008). Causes and impacts of the 2005 Amazon drought. *Environmental Research Letters*, *3*(1). https://doi.org/10.1088/1748-9326/3/1/014002

Zhang, Y., Chiessi, C. M., Mulitza, S., Sawakuchi, A. O., Häggi, C., Zabel, M., et al. (2017). Different precipitation patterns across tropical South America during Heinrich and Dansgaard-Oeschger stadials. *Quaternary Science Reviews*, *177*, 1–9. https://doi.org/10.1016/j.quascirev.2017.10.012

References From the Supporting Information

Björck, S., & Wohlfarth, B. (2002). 14C Chronostratigraphic techniques in paleolimnology. In W. M. Last, & J. P. Smol (Eds.), *Tracking environmental change using lake sediments*, *Developments in Paleoenvironmental Research*, (Vol. 1, Chapterd 10, 205–245). Dordrecht: Springer.

Blaauw, M., & Christen, J. A. (2011). Flexible paleoclimate age-depth models using an autoregressive gamma process. *Bayesian Analysis*, *6*(3), 457–474. https://doi.org/10.1214/11-BA618

Haug, G. H., Hughen, K. A., Sigman, D. M., Peterson, L. C., & Röhl, U. (2001). Southward migration of the intertropical convergence zone through the Holocene. *Science*, *293*(5533), 1304–1308. https://doi.org/10.1126/science.1059725

Hedges, J. I., Clark, W. A., Quay, P. D., Richey, J. E., Devol, A. H., & Santos, M. (1986). Compositions and fluxes of particulate organic material in the Amazon River1. *Limnology and Oceanography*, *31*(4), 717–738. https://doi.org/10.4319/lo.1986.31.4.0717

INMET. (2019). Instituto Nacional de Metereologia. Retrieved in May 10, 2019 from http://www.inmet.gov.br/.

Kang, S. M., Held, I. M., Frierson, D. M., & Zhao, M. (2008). The response of the ITCZ to extratropical thermal forcing: Idealized slab-ocean experiments with a GCM. *Journal of Climate*, *21*(14), 3521–3532. https://doi.org/10.1175/2007JCLI2146.1

Mayorga, E., Aufdenkampe, A. K., Masiello, C. A., Krusche, A. V., Hedges, J. I., Quay, P. D., et al. (2005). Young organic matter as a source of carbon dioxide outgassing from Amazonian rivers. *Nature*, *436*(7050), 538–541. https://doi.org/10.1038/nature03880

Reimer, P. J., Bard, E., Bayliss, A., Beck, J. W., Blackwell, P. G., Bronk Ramsey, C., et al. (2013). IntCal13 and Marine13 radiocarbon age calibration curves 0–50,000 years cal BP. *Radiocarbon*, *55*(4), 1869–1887. https://doi.org/10.2458/azu_js_rc.55.16947

SENAMHI. (2019). Servicio Nacional de Meteorología e Hidrología del Perú. Retrieved in May 10, 2019 from http://www.senamhi.gob.pe.

van Hengstum, P. J., Donnelly, J. P., Fall, P. L., Toomey, M. R., Albury, N. A., & Kakuk, B. (2016). The intertropical convergence zone modulates intense hurricane strikes on the western North Atlantic margin. *Scientific Reports*, *6*(1), 21728. https://doi.org/10.1038/srep21728